Photochemistry and Photobiology, 2007, 83: 1034–1039

Photodynamic Therapy of Vertebral Metastases: Evaluating Tumor-to-Neural Tissue Uptake of BPD-MA and ALA-PpIX in a Murine Model of Metastatic Human Breast Carcinoma†

Margarete K. Akens*[1], Albert J. M. Yee[1], Brian C. Wilson[2], Shane Burch[3], Crystal L. Johnson[2], Lothar Lilge[2] and Stuart K. Bisland[2]

[1]Division of Orthopaedic Surgery, Sunnybrook Health Sciences Centre, Toronto, Ontario, Canada
[2]Department of Biophysics and Bioimaging, Ontario Cancer Institute, University Health Network, Toronto, Ontario, Canada
[3]Department of Orthopaedic Surgery, University of California, San Francisco, CA

Received 12 January 2007; accepted 24 April 2007; DOI: 10.1111/j.1751-1097.2007.00172.x

ABSTRACT

Photodynamic therapy has been successfully applied to numerous cancers. Its potential to treat cancer metastases in the spine has been demonstrated previously in a preclinical animal model. The aim of this study was to test two photosensitizers, benzoporphyrin-derivative monoacid ring A (BPD-MA) and by 5-aminolevulinic acid (5-ALA)-induced protoporphyrin IX (PpIX), for their potential use to treat bony metastases. The difference in photosensitizer concentration in the spinal cord and the surrounding tumor-bearing vertebrae was of particular interest to assess the risk of potential collateral damage to the spinal cord. Vertebral metastases in a rat model were generated by intracardiac injection of human breast cancer cells. When tumor growth was confirmed, photosensitizers were injected systemically and the animals were euthanized at different time points. The following tissues were harvested: liver, kidney, ovaries, appendicular bone, spinal cord and lumbar vertebrae. Photosensitizer tissue concentration of BPD-MA or PpIX was determined by fluorescence spectrophotometry. In contrast to BPD-MA, ALA-PpIX did not demonstrate an appreciable difference in the uptake ratio in tumor-bearing vertebrae compared to spinal cord. The highest ratio for BPD-MA concentration was found 15 min after injection, which can be recommended for therapy in this model.

INTRODUCTION

Photodynamic therapy (PDT) has been applied successfully to various cancers, including brain neoplasms, recurrent breast carcinoma, esophagus and lung carcinoma (1–4). There is recent interest in the potential application of PDT to treat bony lesions, with reported studies in established preclinical animal models (5,6). In particular, metastatic lesions to bone are of interest, given its increasing prevalence, due in part to improvements in adjuvant therapies. Thus, the use of bisphosphonate medical therapy in breast carcinoma has contributed toward a decline in age-standardized breast cancer mortality, resulting in a greater proportion of patients who are living longer with advanced metastatic bony spread (7). The key clinical complication is skeletally related events (SREs) that result in bony pain and fracture, including spinal instability with neurologic dysfunction related to neurologic compression by pathologic bony elements (8). SREs involving vertebral metastases significantly impact quality of life (9). There are limitations to current local therapies directed at treating vertebral metastases, in particular the local radiation therapy dose that can be applied to the spinal neural elements while avoiding radiation-induced myelopathy. In addition, spinal surgery following prior radiation therapy is associated with a three- to four-fold increase in wound complication rates (10). PDT may be a useful neoadjunct approach in the treatment of vertebral metastases coupled with spinal surgical techniques such as vertebroplasty (PV) or kyphoplasty. An advantage would be to combine a biologic ablative local therapy such as PDT with the objective of vertebral stabilization afforded by PV and kyphoplasty (6).

In PDT, light of a specific wavelength is administered to a target tissue containing a photosensitizing agent. The light activation generates a photochemical reaction that leads to the generation of reactive oxygen species, mainly singlet oxygen (11), which is cytotoxic and causes destruction of the tumor cells and/or tumor neovasculature. There are several photosensitizers available, with varying effects that relate to the mechanism(s) of action, the applied drug dose, drug–light interval and locally applied light energy. The ability to define closely the window of maximum therapeutic efficacy in vertebral PDT, without collateral damage to the neural elements, has been highlighted by Burch *et al.* (6) in a preclinical animal study. As such, bony tumor-to-neural tissue selectivity of photosensitizer is critical (12). The purpose of the present study was to compare two clinical photosensitizers, benzoporphyrin-derivative monoacid ring A (BPD-MA) and 5-aminolevulinic acid (5-ALA)-induced endogenous protoporphyrin IX (PpIX), evaluating their tumor-to-neural tissue selectivity using an established osteolytic murine model of metastatic human breast carcinoma. BPD-MA, in a liposomal formulation (Visudyne®), is used clinically for the treatment of neovascularization caused by age-related macular degeneration (13). Administration of

†This invited paper is part of the Symposium-in-Print: Photodynamic Therapy.
*Corresponding author email: makens@uhnres.utoronto.ca (Margarete K. Akens)

5-ALA increases intracellular production of PpIX, a precursor of heme, that possesses photosensitizing activity. PDT using 5-ALA has been reported in several dermatological and gastroenterological applications (14).

The photosensitizer tissue concentration of BPD-MA and 5-ALA-induced PpIX was determined at different time points to define the optimal drug–light treatment time based on organ specific uptake. The difference in photosensitizer tissue concentration between the spinal cord and the surrounding vertebrae was of particular interest, because this could determine the risk of potential collateral damage to the spinal cord while maintaining PDT efficacy to targeted tumor.

MATERIALS AND METHODS

Animal model. Following institutional approval (University Health Network, Toronto, Canada), vertebral metastases were generated by injection of human breast cancer carcinoma cells (MT-1) into 5–8 week old female nude rats (rnu/rnu; Harlan Sprague–Dawley, Indianapolis, IN). The injected MT-1 cells were stably transfected with the luciferase gene (6). Seventy-nine rats were randomly allocated to different treatment and control groups (Table 1). In animals of the tumor group (Table 1, column 3), 2×10^6 cells in 200 μL RPMI 1640 media were injected under general anesthesia (2% isofluorane/2L O_2) into the left heart ventricle using a 1 mL syringe with a 25 g needle. Pulsatile blood within the needle cone confirmed the correct position of the needle. The animals were immediately recovered and returned to their cages with free access to standard food and water. Fifteen days later *in vivo* bioluminescence imaging confirmed the establishment of metastases. For this luciferin (Xenogen Corp., Alameda, CA) was dissolved in 0.9% sodium chloride solution at a concentration of 30 and 60 mg kg^{-1} was injected intraperitoneally to anesthetized animals. Five minutes later the bioluminescent signal was acquired using an IVIS Bioluminescent Imaging system (Xenogen Corp.). Images of each rat were taken in the left lateral and ventral positions. Rats with bioluminescence-confirmed metastases were subsequently injected intravenously with photosensitizers. The animals were euthanized at specified time points according to experimental group. Nontumor cell injected rats (Table 1, column 4), were also injected with photosensitizer. Additional control animals without drug injection were evaluated for baseline endogenous PpIX production.

Photosensitizers. BPD-MA (QLT, Vancouver, BC, Canada) was used at a dose of 2 mg kg^{-1} and dissolved in 200 μL 5% dextrose. This BPD-MA is commercially available as Visudyne® (Novartis, Canada). 5-ALA (Sigma-Aldrich, Oakville, ON, Canada) was administered at 10, 50 or 200 mg kg^{-1}. The drug was dissolved in PBS, pH adjusted to 7.2 with 1 M NaOH (15). Both photosensitizers were injected intravenously. The rats were euthanized by barbiturate overdose (120 mg kg^{-1} Euthanol®; Bimeda-MTC, Cambridge, ON, Canada) at different time points. The following tissues were harvested and snap frozen in liquid nitrogen for subsequent determination of the photosensitizer concentration analysis: liver, kidney, ovaries, spinal cord, lumbar vertebrae, femura and/or humeri (bone). Muscles surrounding the vertebrae were excised and the spinal cord, including the dura mater spinalis, was removed from the spinal canal and stored separately at −80°C in the dark. Four to five vertebrae, including the intervertebral discs, were minced as a single sample directly prior to analyses. Vertebrae producing a positive bioluminescence signal (TIV: tumor-involved vertebrae) were included in the tissue harvest. For two reasons it was not possible to separate TIV from nontumor-bearing vertebrae (non-TIV); firstly, the tumor must reach a certain size to be detected by bioluminescence and, secondly, the tumor is macroscopically not visible and cannot be detected with other methods without interfering with the measurement of the photosensitizer concentration. Figure 1 shows a typical distribution of the tumor within a lumbar vertebra. The decalcified tissue section is stained with mouse anti-human epidermal growth factor receptor antibody (Zymed®Laboratories Inc., San Francisco, CA), which does not show cross reactivity to rat tissues, to distinguish the tumor from bone and bone marrow.

Tissue analyses. The tissue was analyzed for BPD-MA and PpIX concentration using a solubilization technique described previously (16). Prior to measuring the photosensitizer tissue concentration, a spiking experiment was repeated. A concentration of 250 μg g^{-1} BPD-MA were added to a sample, which was measured six times and showed the anticipated results (244.4 ± 24.6 μg g^{-1}). Following this, the photosensitizer uptake in tissue samples was measured, for which tissue was first thawed, morsellized and then incubated in 2 mL Solvable™ (Packard BioScience BV, Groningen, The Netherlands) for 1 h in a water bath at 50°C. The sample was then mechanically homogenized (Tissue Tearor, Biospec Products Inc., Racine, WI) in the same vial. A fixed amount (0.2 mL) of the homogenate was transferred into a new vial containing 1 mL Solvable™ and 3 mL of dH_2O and then incubated for 1 h at 50°C. The optical density (OD) was measured in a spectrophotometer at the appropriate drug excitation wavelength (415 nm for BPD-MA and 401 nm for PpIX) and reduced to below 0.1 by a known dilution factor with dH_2O. The fluorescence spectrophotometer (Photon Technologies Industries [PTI], London, ON, Canada) was

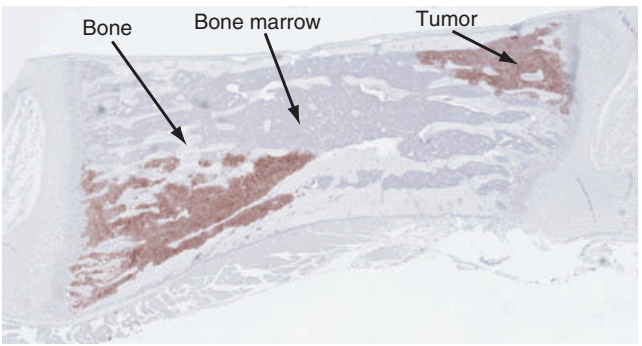

Figure 1. Typical distribution of the tumor within a lumbar vertebra. The decalcified tissue section is stained with mouse anti-human epidermal growth factor receptor antibody (dark color that highlights the tumor).

Table 1. Number of animals in each study group.

Photosensitizer	Dose (mg kg^{-1})	Tumor-bearing rats	Healthy rats	Time points
BPD-MA	2	30	12	15 min, 1 h, 3 h, 24 h
5-ALA/PpIX	200	19	3*	2 h, 4 h, 6 h, 2 h* only
5-ALA/PpIX	50	3		2 h
5-ALA/PpIX	10	3		2 h
No drug		3	6	

The 3 healthy rats were measured only at the 2 h time point compared to the tumor-bearing rats, which were measured at 2 h, 4 h and 6 h time points.
BPD-MA, benzoporphyrin derivative monoacid ring A; 5-ALA, 5-aminolevulinic acid; PpIX, protoporphyrin IX.

calibrated for absolute BPD-MA and PpIX concentration using a dilution series of the photosensitizer treated identically with Solvable™. Each sample was repeated in triplicate and standardized to tissue weight. The photosensitizer concentration (C_t) in the tissue was calculated according to:

$$C_t = \frac{S_n}{\alpha_{ps}} \frac{(V_t + V_s)}{V_t} \frac{4.2}{0.2} D.$$

For all samples, a normalized signal (S_n) was calculated as the ratio of the sample count rate over the crystal count rate. A photobleaching resistant, solid-state dysprosium:YAG crystal (PTI) was used to calibrate the spectrofluorometer. The fluorometer responsivity α_{PS} was calculated from the standard curve of each photosensitizer. The last three factors account for the dilution of the sample at each step, namely mixing of the solid sample V_t (volume tissue) with V_s (volume solvable™), dilution of the 0.2 mL aliquots to 4.2 mL total volume and adjustment of the OD if required (16). The excitation wavelength to measure BPD-MA was 415 nm and the emission spectrum was collected from 600–750 nm and the peak centered at 690 nm integrated with autofluorescence subtraction. For PpIX, the corresponding wavelength were 401 and 600–720 nm (peak at 635 nm). The concentration ratio between vertebral bone and spinal cord was calculated for each animal and the mean ratios compared among different time intervals by ANOVA analysis. A power/sample size calculation was performed on preliminary data obtained from samples of rats treated with BPD-MA, with the tissues harvested at 15 min postdrug administration. Based upon a calculated standard deviation of 0.36 of the mean values for the ratio (vertebral bone:spinal cord photosensitizer uptake), and assuming a beta of 0.20 (power = $1-\beta$ = 0.8) with alpha set at 0.05, it was estimated that approximately four animals per drug group would be required at each time interval to detect a 25% difference between the two drugs in the ratio of vertebral bone to spinal cord photosensitizer levels. Statistical significance was set at $P < 0.05$. In addition, mean values of vertebral bone and spinal cord photosensitizer uptake were compared between tumor-bearing and normal rats.

RESULTS

Animal model

Of the rats injected with tumor cells, one died within 24 h of injection. Of the 78 surviving rats, 96% were bioluminescence positive at 15 days following injection (Fig. 2). Bone metastases were observed in 78% of these (68% vertebral, 60% femoral). Ovarian tumors were observed in 52%.

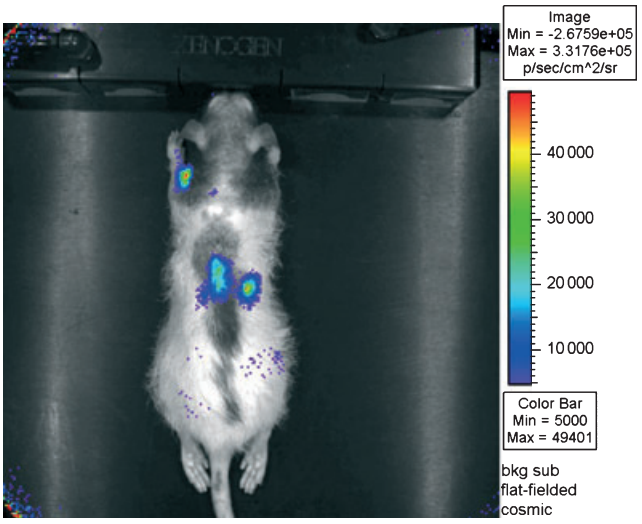

Figure 2. Bioluminescent image of a rat in dorsoventral position 15 days following tumor cell injection. The colored areas represent the luciferase transfected MT-1 carcinoma cells.

Photosensitizer tissue concentration

BPD-MA. Detectable drug levels were observed in all tissue samples at 15 min, 1 h and 3 h following BPD-MA injection in both tumor-bearing and control animals. The highest concentration was in the liver, followed by the kidney, ovary, vertebra and appendicular bone (Fig. 3a). Consistent with these results, Richter *et al.* (17) also reported the highest BPD-MA concentration in the liver, followed by the kidney. The photosensitizer was equally distributed throughout the liver and kidney, for which there was sufficient tissue to analyze up to three samples and the intrasample variability was small (< 10%). Additionally, the interanimal variation of photosensitizer concentration was lower in liver and kidney than in the bony vertebrae. The lowest concentration at all time points was in the spinal cord (Fig. 3b). In general, for all tissues the highest concentrations were found between 15 min and 1 h and decreased thereafter (Fig. 3a,b). Tumor-bearing tissues contained higher levels of BPD-MA compared to nontumor control animals (Fig. 3b). This was statistically significant at 15 min ($P < 0.05$) and 24 h ($P < 0.05$) and showed a trend at 1 ($P = 0.09$) and 3 h

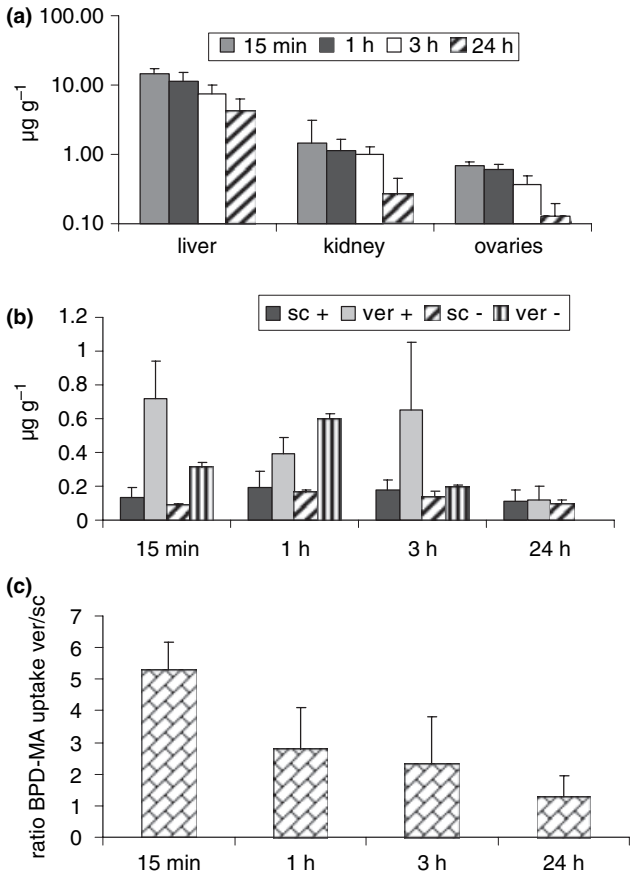

Figure 3. Tissue concentration of (a) BPD-MA concentration in liver, kidney and ovaries of tumor-bearing rats and (b) BPD-MA (2 mg kg^{-1}) in the spinal cord (sc) and vertebrae (ver) of tumor-bearing (+) and healthy (−) rats. (c) BPD-MA uptake ratio between tumor-bearing vertebrae and spinal cord at different time points. Error bars represent SD on the means.

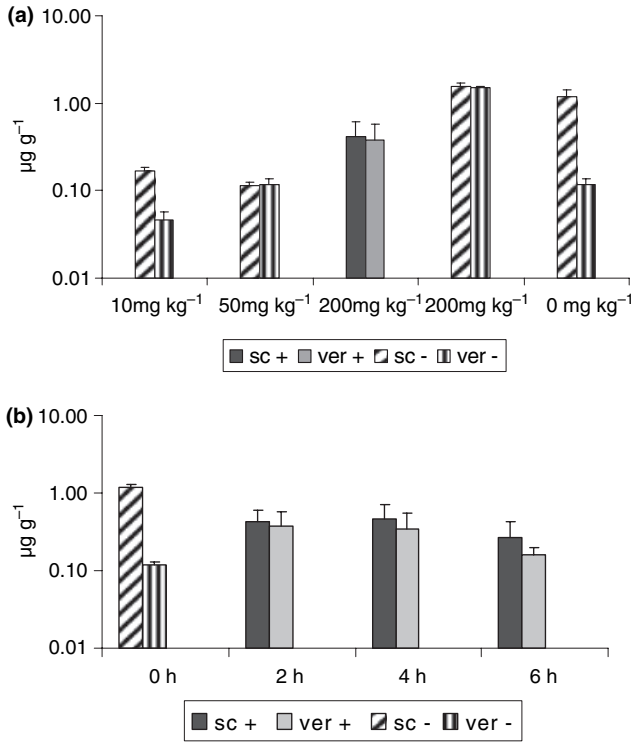

Figure 4. (a) PpIX concentration in the spinal cord (sc) and vertebrae (ver) in tumor-bearing (+) and healthy (–) rats at 2 h after different doses of 5-ALA. (b) PpIX (200 mg kg^{-1} 5-ALA) in spinal cord (sc) and vertebrae (ver) of tumor-bearing (+) rats at different time points.

($P = 0.09$). In the animals with bony metastases, the highest tumor-to-neural tissue photosensitizer concentration was at 15 min, at which time the TIV concentrations were on average 5.5-fold greater than spinal cord levels. This ratio was statistically higher than the values at 1 ($P < 0.05$), 3 ($P < 0.01$) and 24 h ($P < 0.001$) (Fig. 3c). In non-TIV the BPD-MA level was, on average, 3.4-fold greater than spinal cord levels at 15 min.

PpIX. The highest concentration of PpIX was observed in the kidney, followed by the liver, spinal cord and ovaries. The concentration in normal control rats was 9.4-fold greater in the spinal cord than in the vertebrae. Two hours after 5-ALA injection, the PpIX tissue concentration increased in the vertebrae, but it was still 2.7-fold greater in the spinal cord at 10 mg kg^{-1} than in the vertebral bone. At 50 and 200 mg kg^{-1} this difference was still 1.3- and 1.4-fold, respectively (Fig. 4a). In the tumor-bearing animals the photosensitizer concentration in the vertebrae also increased with administered 200 mg kg^{-1} 5-ALA dose, but never exceeded these values measured in the spinal cord (Fig. 4b). The PpIX concentrations decreased slightly over time (2, 4 and 6 h) in the tumor-bearing vertebrae and the spinal cord, but never exceeded the concentrations measured in the spinal cord. The PpIX concentration in the vertebrae of healthy rats at the 2 h time point was comparable to the endogenous phorphyrin level found in the spinal cord (Table 2). Overall, it was not possible to observe any indication of elevated PpIX production in the vertebrae above the endogenous level in the spinal cord. Hence, we abstained from measuring PpIX production in tumor-bearing rats to minimize animal use.

Table 2. Ratio of PpIX concentration between the spinal cord and vertebrae.

5-ALA/time interval	Tumor confirmed by bioluminescence	Uptake ratio, spinal cord/vertebrae
0 mg	Negative	9.4 ± 3.3
10 mg 2 h^{-1}	Positive	2.7 ± 1.2
50 mg 2 h^{-1}	Positive	1.3 ± 0.4
200 mg 2 h^{-1}	Negative	1.0 ± 0.2
200 mg 2 h^{-1}	Positive	1.4 ± 0.8
200 mg 4 h^{-1}	Positive	1.4 ± 0.7
200 mg 6 h^{-1}	Positive	1.6 ± 0.9

PpIX, protoporphyrin IX; 5-ALA, 5-aminolevulinic acid.

DISCUSSION

Anatomically, the bony vertebrae surround the spinal cord, so that the latter may be at risk of collateral damage in PDT treatment of vertebral lesions. This is of particular concern, as the light fluence field may not be tailored to completely exclude the spinal cord. Ideally, a photosensitizer for vertebral PDT should accumulate at higher concentrations in tumor tissue than the surrounding normal tissue (17). Selecting the optimal drug–light interval for applying vertebral PDT will depend, in part, on achieving high uptake in the tumor-bearing vertebrae and on high tumor-to-neural tissue selectivity, for treatment efficacy and safety, respectively. The concentration of BPD-MA was higher at all time points in vertebrae from animals with established bony metastases than control animals. The metastases in this model were typically located within the cancellous bone of the vertebral body and were found both cranially and caudally close to the growth plates. At later stages the entire vertebrae are filled with tumor tissue and the cortical bone can also be involved.

Clinically, BPD-MA has been used to target neovasculature in ocular macular degeneration at 15 min following drug administration (13). Using a BPD-MA concentration of 2 mg kg^{-1} the highest increase (three- to five-fold) in vertebral bone to spinal cord uptake was also observed at 15 min. This ratio in healthy rats was the same as seen in a pilot study in healthy dogs. However, the absolute tissue concentration between these two species varied: the BPD-MA concentration in the canine spinal cord was 3.8-fold higher than in the rat at 15 min, which appears to be the best time interval for vertebral PDT in this model. The concentration in the kidneys was similar in both species, while the dog liver showed only half the uptake as the rat liver. The species-specific differences merit further investigation, as they suggest that there may be differences between values in rat and human. Nevertheless, it can be speculated that, as the ratio of vertebrae-to-spinal cord tissue concentration is close to unity in two distinct species, it may be similar in humans as well.

Species-specific differences in uptake and a different technique to analyze tissue concentration used does not allow direct comparison of results from this study with published values (17,18) Richter *et al.* (17) injected radioactively labeled BPD-MA to measure the tissue distribution in mice, in contrast to the spectofluoroscopy used here to determine the concentration in rat tissue. These methods have not been validated against each other (18). Photobleaching is not a concern when using radioactively labeled photosensitizer.

However, although bleaching may occur when using the solubilization technique, it is important to note that the instrument calibration was also executed under the same conditions, and thus bleaching associated error become negligible. Additionally, it will not significantly affect the uptake ratios between the vertebrae and spinal cord, since any effect will largely cancel. A second potential source of error in the measurement is that tissue photosensitizer concentrations could have been overestimated due to aggregate formation (19). However, BPD-MA is prepared in a lipid-base formulation to minimize aggregate formation (20). PpIX does not form aggregates.

No appreciable differences were observed in vertebral bone *versus* spinal cord uptake for 5-ALA at any dose or time interval. The reported PpIX distribution in tissues is consistent with that observed here in our control animals that did not receive 5-ALA (21); the highest concentration was observed in the kidney followed by the liver (22).

In control animals that did not receive either tumor cell injection or 5-ALA, porphyrin tissue concentrations were nine-fold greater in spinal cord than normal vertebral bone. A low endogenous porphyrin concentration in bone is consistent with the findings of van den Boogert *et al.* (22), who showed that tissues of mesodermal origin (*e.g.* bone, muscle) synthesize less ALA-induced PpIX than tissues of ectodermal origin (*e.g.* nervous tissue) or malignant tissue. Furthermore, the ratio between cells and extracellular matrix is different in bone and spinal cord, with bone containing more extracellular matrix. In addition, there are differences in PpIX synthesis within central nervous tissue. The gray matter appears to produce a significantly higher level of PpIX than white matter, which may be due in part to a lower tissue density of mitochondria in the latter (15,23). The difference in PpIX production between white and gray matter of the spinal cord was confirmed here by fluorescence microscopy. However, the tissue could not easily be separated for spectrofluorometric analyses. As anticipated, the concentration of PpIX increased in the vertebrae with increasing doses of 5-ALA (Fig. 4), but was never above that in the spinal cord.

Tumor treatment using 5-ALA appears successful for other oncologic applications, in part due to malignant tissues possessing a greater capacity to produce PpIX compared to normal tissue at any dose (24). ALA has also been used successfully in photodynamic diagnosis to remove spinal ependymoma using fluorescence-guided resection (25). However, the present study indicates a potential severe limitation to this approach in the spine. Further study comparing various cancer cell types metastasized to the spine might be useful but, *a priori*, is not likely to be significantly different from the findings here.

The PpIX concentration measured by Gabeler *et al.* (26) in rat arteries was done using a fluorimetric enzyme assay, also normalizing the PpIX concentration to the protein content. In that study the focus was on the absolute values in the spinal cord and vertebrae and not the relative concentration. The lower absolute PpIX concentration in the spinal cord and vertebrae samples in some may be due to the length and method of tissue storage as PpIX content may decrease over time (27), and a pilot study revealed a slightly greater variability in PpIX concentration in frozen compared to fresh tissue, but this was not statistically significant. However, the vertebrae and spinal cord tissue of the each rat were stored and analyzed together. The absolute endogenous PpIX concentration appears to vary among species. In a pilot study porcine and murine spinal cord had a 6.7-fold higher endogenous PpIX concentration compared to canine spinal cord, but similar levels in the bone. In the rat it was not possible to increase the PpIX production in the vertebrae above the spinal cord level after 5-ALA administration, which may explain why PpIX cannot be recommended as a photosensitizer to treat metastases in the murine spine. However, this was not tested in other species.

Establishment of bony metastases was confirmed by bioluminescence at 15 days following tumor cell injection (28,29). Because of the small size of a single rat vertebrae, four to five were harvested together for photosensitizer quantification. For PDT the results need to be considered in the context of the aggregate analyses performed, which included several vertebrae with various bioluminescent signals and, hence, relative tumor burden. This may explain the higher variability in the vertebrae results compared to other tissues. Additionally, the vertebrae are intrinsically heterogeneous; it was not possible to separate the bone from the bone marrow and tumor, and it is more challenging to prepare the tissue due to the hardness of the bone.

The clinical scenario of a stereotactic localization to a single vertebral level of interest (*i.e.* high tumor burden) may provide a higher tumor to nontumor photosensitizer tissue concentration than in this study, where vertebrae with different tumor burden were analyzed together. Photosensitizers exert their effects through a variety of mechanisms, which include directly targeting the tumor cells and targeting the tumor neovasculature. Given the photosensitizer measurement technique, the present study was not able to discern the uptake in different microarchitectural tumor compartments. The time point selected may not be the optimum, if the subcellular localization in vertebrae and spinal cord differ at this time.

In summary, the present study indicates an appreciable difference in BPD-MA drug uptake between murine TIV and spinal cord tissue, which is desirable in intravertebral PDT. 5-ALA-induced PpIX did not demonstrate this necessary effect, using the photosensitizer range and time intervals evaluated, which are in the clinically realistic range. This raises a significant concern for high spinal cord levels. Ongoing studies in larger animal models evaluating both drug and light dosimetry are required in guiding the choice of an ideal photosensitizer in clinical PDT of vertebral metastases with primary outcomes of efficacy and safety.

Acknowledgements—This work was supported by the Canadian Breast Cancer Foundation, Ontario Chapter. The tissue extraction assays were supported by NIH Program Project Grant CA 43892. The human breast cancer MT-1 cells were kindly provided by Dr. O. Engebraaten, Norwegian Radium Hospital, Oslo, Norway.

REFERENCES

1. Powers, S. K., S. S. Cush, D. L. Walstad and L. Kwock (1991) Stereotactic intratumoral photodynamic therapy for recurrent malignant brain tumors. *Neurosurgery* **29**, 688–695.
2. Marcon, N. E. (1994) Photodynamic therapy and cancer of the esophagus. *Semin. Oncol.* **21**, 20–23.

3. Lam, S. (1994) Photodynamic therapy of lung cancer. *Semin. Oncol.* **21**, 15–19.
4. Allison, R., T. Mang, G. Hewson, W. Snider and D. Dougherty (2001) Photodynamic therapy for chest wall progression from breast carcinoma is an underutilized treatment modality. *Cancer* **91**, 1–8.
5. Burch, S., A. Bogaards, J. Siewerdsen, D. Moseley, A. Yee, J. Finkelstein, R. Weersink, B. C. Wilson and S. K. Bisland (2005a) Photodynamic therapy for the treatment of metastatic lesions in bone: Studies in rat and porcine models.. *J. Biomed. Opt.* **10**, 034011.
6. Burch, S., S. K. Bisland, A. Bogaards, A. J. Yee, C. M. Whyne, J. A. Finkelstein and B. C. Wilson (2005b) Photodynamic therapy for the treatment of vertebral metastases in a rat model of human breast carcinoma. *J. Orthop. Res.* **23**, 995–1003.
7. Tatsui, H., T. Onomura, S. Morishita, M. Oketa and T. Inoue (1996) Survival rates of patients with metastatic spinal cancer after scintigraphic detection of abnormal radioactive accumulation. *Spine* **21**, 2143–2148.
8. Ecker, R. D., T. Endo, N. M. Wetjen and W. E. Krauss (2005) Diagnosis and treatment of vertebral column metastases. *Mayo Clin. Proc.* **80**, 1177–1186.
9. Weigel, B., M. Maghsudi, C. Neumann, R. Kretschmer, F. J. Muller and M. Nerlich (1999) Surgical management of symptomatic spinal metastases. Postoperative outcome and quality of life. *Spine* **24**, 2240–2246.
10. Wai, E. K., J. A. Finkelstein, R. P. Tangente, L. Holden, E. Chow, M. Ford and A. Yee (2003) Quality of life in surgical treatment of metastatic spine disease. *Spine* **28**, 508–512.
11. Niedre, M., M. S. Patterson and B. C. Wilson (2002) Direct near-infrared luminescence detection of singlet oxygen generated by photodynamic therapy in cells in vitro and tissues in vivo. *Photochem. Photobiol.* **75**, 382–391.
12. Bourre, L., N. Rousset, S. Thibaut, S. Eleouet, Y. Lajat and T. Patrice (2002) PDT effects of m-THPC and ALA, phototoxicity and apoptosis. *Apoptosis* **7**, 221–230.
13. Bressler, N. M. (2001) Photodynamic therapy of subfoveal choroidal neovascularization in age-related macular degeneration with verteporfin: Two-year results of 2 randomized clinical trials-tap report 2. *Arch. Ophthalmol.* **119**, 198–207.
14. Kelty, C. J., N. J. Brown, M. W. Reed and R. Ackroyd (2002) The use of 5-aminolaevulinic acid as a photosensitiser in photodynamic therapy and photodiagnosis. *Photochem. Photobiol. Sci.* **1**, 158–168.
15. Olivo, M. and B. C. Wilson (2004) Mapping ALA-induced PPIX fluorescence in normal brain and brain tumour using confocal fluorescence microscopy. *Int. J. Oncol.* **25**, 37–45.
16. Lilge, L., C. O'Carroll and B. C. Wilson (1997) A solubilization technique for photosensitizer quantification in ex vivo tissue samples. *J. Photochem. Photobiol. B, Biol.* **39**, 229–235.
17. Richter, A. M., S. Cerruti-Sola, E. D. Sternberg, D. Dolphin and J. G. Levy (1990) Biodistribution of tritiated benzoporphyrin derivative (3H-BPD-MA), a new potent photosensitizer, in normal and tumor-bearing mice. *J. Photochem. Photobiol. B, Biol.* **5**, 231–244.
18. Bland, J. M. and D. G. Altman (1986) Statistical methods for assessing agreement between two methods of clinical measurement. *Lancet* **1**, 307–310.
19. Pogue, B. W., X. D. Zhou, S. Gibbs, S. Davis, D. Kepshire, K. D. Paulsen and T. Hasan (2006) Comparison of techniques for quantification of fluorescence from tissue—art. no. 61390N. In *Optical Methods for Tumor Treatment and Detection: Mechanisms and Techniques in Photodynamic Therapy XV* (Edited by D. Kessel), pp. 135–147. Proceedings of the Society of Photo-Optical Instrumentation Engineers (SPIE).
20. Chowdhary, R. K., I. Sharif, N. Chansarkar, D. Dolphin, L. Ratkay, S. Delaney and H. Meadows (2003) Correlation of photosensitizer delivery to lipoproteins and efficacy in tumor and arthritis mouse models; comparison of lipid-based and Pluronic P123 formulations. *J. Pharm. Pharm. Sci.* **6**, 198–204.
21. Uehlinger, P., M. Zellweger, G. Wagnieres, L. Juillerat-Jeanneret, H. van den Bergh and N. Lange (2000) 5-Aminolevulinic acid and its derivatives: Physical chemical properties and protoporphyrin IX formation in cultured cells. *J. Photochem. Photobiol. B, Biol.* **54**, 72–80.
22. van den Boogert, J., R. van Hillegersberg, F. W. de Rooij, R. W. de Bruin, A. Edixhoven-Bosdijk, A. B. Houtsmuller, P. D. Siersema, J. H. Wilson and H. W. Tilanus (1998) 5-Aminolaevulinic acid-induced protoporphyrin IX accumulation in tissues: Pharmacokinetics after oral or intravenous administration. *J. Photochem. Photobiol. B, Biol.* **44**, 29–38.
23. Lilge, L. and B. C. Wilson (1998) Photodynamic therapy of intracranial tissues: A preclinical comparative study of four different photosensitizers. *J. Clin. Laser. Med. Surg.* **16**, 81–91.
24. Pottier, R. H. and J. C. Kennedy (1996) Photodynamic therapy with 5-aminolevulinic acid: Basic principles and applications. *Proc. Soc. Photo. Opt. Instrum. Eng.* **2625**, 2–10.
25. Arai, T., S. Tani, A. Isoshima, H. Nagashima, T. Joki, J. Takahashi-Fujigasaki and T. Abe (2006) Intraoperative photodynamic diagnosis for spinal ependymoma using 5-aminolevulinic acid: Technical note. *No Shinkei Geka* **34**, 811–817.
26. Gabeler, E. E., W. Sluiter, R. van Hillegersberg, A. Edixhoven, K. Schoonderwoerd, R. G. Statius van Eps and H. van Urk (2003) Aminolaevulinic acid-induced protoporphyrin IX pharmacokinetics in central and peripheral arteries of the rat. *Photochem. Photobiol.* **78**, 82–87.
27. Nuttall, K. L. (1996) Porphyrins and disorders of porphyrin metabolism. In *Tietz Fundamentals of Clinical Chemistry* (Edited by C. A. Burtis and E. R. Ashwood), pp. 731–744. W. B. Saunders Company, Philadelphia.
28. Rice, B. W., M. D. Cable and M. B. Nelson (2001) In vivo imaging of light-emitting probes. *J. Biomed. Opt.* **6**, 432–440.
29. Nogawa, M., T. Yuasa, S. Kimura, J. Kuroda, K. Sato, H. Segawa, A. Yokota and T. Maekawa (2005) Monitoring luciferase-labeled cancer cell growth and metastasis in different in vivo models. *Cancer Lett.* **217**, 243–253.